Original Article

A nomogram based on dual-layer detector spectral computed tomography quantitative parameters and morphological quantitative indicator for distinguishing metastatic and nonmetastatic regional lymph nodes in pancreatic ductal adenocarcinoma

Youjia Wen, Zuhua Song, Qian Li, Dan Zhang, Xiaojiao Li, Qian Liu, Jiayi Yu, Zongwen Li, Xiaofang Ren, Jiayan Zhang, Dan Zeng, Zhuoyue Tang

Department of Radiology, Chongqing General Hospital, Chongqing, China

Contributions: (I) Conception and design: Y Wen, Z Song; (II) Administrative support: Z Tang; (III) Provision of study materials or patients: Q Li, D Zhang, X Li, Q Liu; (IV) Collection and assembly of data: J Yu, Z Li, X Ren, J Zhang, D Zeng; (V) Data analysis and interpretation: Y Wen, Z Song; (VI) Manuscript writing: All authors; (VII) Final approval of manuscript: All authors.

Correspondence to: Zhuoyue Tang, PhD. Department of Radiology, Chongqing General Hospital, No. 118, Xingguang Avenue, Liangjiang New Area, Chongqing 401147, China. Email: zhuoyue_tang@cqmu.edu.cn.

Background: There is no unified scope for regional lymph node (LN) dissection in patients with pancreatic ductal adenocarcinoma (PDAC). Incomplete regional LN dissection can lead to postoperative recurrence, while blind expansion of the scope of regional LN dissection significantly increases the perioperative risk without significantly prolonging overall survival. We aimed to establish a noninvasive visualization tool based on dual-layer detector spectral computed tomography (DLCT) to predict the probability of regional LN metastasis in patients with PDAC.

Methods: A total of 163 regional LNs were reviewed and divided into a metastatic cohort (n=58 LNs) and nonmetastatic cohort (n=105 LNs). The DLCT quantitative parameters and the nodal ratio of the longest axis to the shortest axis (L/S) of the regional LNs were compared between the two cohorts. The DLCT quantitative parameters included the iodine concentration in the arterial phase (APIC), normalized iodine concentration in the arterial phase (APNIC), effective atomic number in the arterial phase (APZeff), normalized effective atomic number in the arterial phase (APNZeff), slope of the spectral attenuation curves in the arterial phase (APλHU), iodine concentration in the portal venous phase (PVPIC), normalized iodine concentration in the portal venous phase (PVPNIC), effective atomic number in the portal venous phase (PVPZeff), normalized effective atomic number in the portal venous phase (PVPNZeff), and slope of the spectral attenuation curves in the portal venous phase (PVPλHU). Logistic regression analysis based on area under the curve (AUC) was used to analyze the diagnostic performance of significant DLCT quantitative parameters, L/S, and the models combining significant DLCT quantitative parameters and L/S. A nomogram based on the models with highest diagnostic performance was developed as a predictor. The goodness of fit and clinical applicability of the nomogram were assessed through calibration curve and decision curve analysis (DCA).

Results: The combined model of APNIC + L/S (APNIC + L/S) had the highest diagnostic performance among all models, yielding an AUC, sensitivity, and specificity of 0.878 [95% confidence interval (CI): 0.825–0.931], 0.707, and 0.886, respectively. The calibration curve indicated that the APNIC-L/S nomogram had good agreement between the predicted probability and the actual probability. Meanwhile, the decision curve indicated that the APNIC-L/S nomogram could produce a greater net benefit than could the all- or-

no-intervention strategy, with threshold probabilities ranging from 0.0 to 0.75.

Conclusions: As a valid and visual noninvasive prediction tool, the APNIC-L/S nomogram demonstrated favorable predictive efficacy for identifying metastatic LNs in patients with PDAC.

Keywords: Pancreatic ductal adenocarcinoma (PDAC); lymph node (LN); dual-layer detector spectral computed tomography (DLCT); nomogram

Submitted Nov 17, 2023. Accepted for publication Apr 30, 2024. Published online May 31, 2024.
doi: 10.21037/qims-23-1624
View this article at: https://dx.doi.org/10.21037/qims-23-1624

Introduction

Pancreatic ductal adenocarcinoma (PDAC), with is associated with an extremely poor prognosis, is expected to be the second most common cause of cancer death worldwide by 2030 (1,2). Most patients with PDAC have lymph node metastasis (LNM) or distant metastasis at the time of diagnosis, and the 5-year survival rate is only about 11 % (3). Surgical resection is still the only remediable treatment strategy for patients with resectable and borderline resectable PDAC (4). LNM is considered to be one of the independent factors influencing the prognosis of PDAC. On the one hand, incomplete regional lymph node (LN) dissection leads to postoperative recurrence (5). On the other hand, blindly expanding the scope of regional LN dissection can significantly increase the perioperative risk via the extension of the operation time, the requirement of intraoperative blood transfusion, and an elevated risk of postoperative complications of patients, all without significantly prolonging overall survival (6,7). The National Comprehensive Cancer Network guidelines recommended preoperative neoadjuvant therapy for patients with LNM, as this can significantly improve survival after surgical resection (8,9). Therefore, accurate preoperative evaluation of LNM in patients with PDAC may be critical to providing individualized treatment options.

The main method for the preoperative evaluation of LNM in PDAC is endoscopic ultrasound, which is an invasive examination that may produce false negatives due to the experience level of the ultrasound diagnostician and the heterogeneity of the lesion (10). Positron emission tomography-computed tomography (PET-CT) has obvious advantages in evaluating the LNM of PDAC; however, it is not recommended as a routine examination for PDAC, and its cost is relatively high, thus limiting its widespread application in clinic (11). Although magnetic resonance imaging provides a degree of accuracy in the identification of metastatic LNs in PDAC (12), several factors restrict its application for determining LN status, including spatial resolution problems, motion artifacts, and dose-dependent oversaturation artifacts (13). Multiphase contrast-enhanced CT is the preferred examination method for the preoperative N staging of PDAC, as it is helpful in evaluating the tumor range, relationship with surrounding blood vessels and organs, and metastasis (14). However, subjectivity is unavoidable when radiologists evaluate the LNM through visual observation, and the sensitivity and accuracy are insufficient to meet the needs of clinical diagnosis. As the existing imaging modalities each possess certain drawbacks in diagnosing metastatic LN in patients with PDAC, a more precise and quantitative diagnostic tool is urgently needed to identify metastatic LNs.

Dual-layer detector spectral CT (DLCT) can provide high- and low-energy X-ray conversion through a dual-layer detector to prevent the mutual interference between different energy rays and guarantee the accuracy of data. The series of energy spectrum images obtained after postprocessing can offer a greater abundance of image features than can conventional CT in contributing to an accurate qualitative and quantitative analysis of substances. Owing to DLCT's particular advantages, emerging DLCT quantitative parameters have been developed and gradually applied for predicting the routine clinical diagnosis of LNM in various cancers including head and neck squamous cell carcinoma, gastric cancer, and rectal cancer, among others (15-18). The nodal ratio of the longest axis to the shortest axis (L/S) has been recommended as a quantification index of metastatic LN morphology (19), as it is more reliable than is the simple short- or long-axis diameter and provides significantly improved sensitivity (20). However, only a few studies have examined the association between DLCT quantitative parameters combined with L/S and LNM in PDAC.

For this study, we hypothesized that DLCT quantitative parameters can aid in identifying the metastatic LNs of

patients with PDAC. To test this, we aimed to build a nomogram combining quantitative parameters and L/S that could identify those patients with PDAC and metastatic regional LN(s). We present this article in accordance with the TRIPOD reporting checklist (available at https://qims.amegroups.com/article/view/10.21037/qims-23-1624/rc).

Methods

Patient and regional LN selection

This study was approved by the Institutional Review Board of the Chongqing General Hospital (No. KY S2022-075-01) and was conducted in accordance with the Declaration of Helsinki (as revised in 2013). The requirement for informed consent was waived due to the retrospective nature the study design. We retrospectively evaluated patients with PDAC who underwent surgical resection with LN dissection at Chongqing General Hospital from September 2021 to December 2022 (n=125). The inclusion criteria for patients were as follows: (I) PDAC was pathologically confirmed, (II) regional LNs were dissected and pathologically examined, and (III) patients underwent contrast-enhanced DLCT examination within two weeks before surgery. Meanwhile, the exclusion criteria for patients were as follows: (I) administration of preoperative neoadjuvant chemotherapy (n=36); (II) quality of image insufficiently high for satisfactory analysis (n=3); (III) complications with other primary malignancies (n=7); and (IV) absence of any clinical, pathological, surgical, or imaging data (n=12). Finally, 67 patients with PDAC were included, among whom 38 were men (61.89±10.59 years) and 29 were women (62.90±9.57 years).

The Japanese Pancreas Society nodal classification of the regional LN stations of the pancreas was used to determine the location of the regional LNs both in radiology and pathology (21). The inclusion criterion for regional LNs was all LNs pathologically confirmed as metastatic or as all nonmetastatic in a given regional LN station. Meanwhile, regional LN stations composed of both pathologically confirmed metastatic and nonmetastatic LNs were excluded.

A total of 163 regional LNs with histological examination were divided into a metastatic LN cohort (n=58) and a nonmetastatic LN cohort (n=105).

DLCT protocol

Contrast-enhanced abdominal scans were performed using a DLCT device (IQon spectral CT, Philips Healthcare, Amsterdam, the Netherlands). All DLCT scans were performed by scanners using a standard protocol, the details of which are described in the Appendix 1.

Matching of the LN stations in the targeted region and quantitative parameter measurements

(I) The matching of the imaging regional LN stations to the pathological ones was completed by two radiologists, with the aim of determining if the targeted regional LN stations were composed of all metastatic or all nonmetastatic LNs. (II) The measurements of the DLCT quantitative parameters and L/S were executed by another two radiologists who were only aware of the targeted regional LN station and not the metastatic status of the targeted regional LN. The DLCT quantitative parameters included iodine concentration in the arterial phase (APIC), normalized iodine concentration in the arterial phase (APNIC), effective atomic number in the arterial phase (APZeff), normalized effective atomic number in the arterial phase (APNZeff), the slope of the spectral attenuation curves in the arterial phase (APλHU), iodine concentration in the portal venous phase (PVPIC), normalized iodine concentration in the portal venous phase (PVPNIC), effective atomic number in the portal venous phase (PVPZeff), normalized effective atomic number in the portal venous phase (PVPNZeff), and the slope of the spectral attenuation curves in the portal venous phase (PVPλHU). Details are described in Appendix 1.

Statistical analysis

All statistical analysis were performed using R software (The R Foundation for Statistical Computing; http://www.R-project.org), SPSS software version 26.0, IBM Corp., Armonk, NY, USA), and MedCalc version 18.2.1 (MedCalc Software, Ostend, Belgium). The Shapiro-Wilk test was used to determine the normality of the data. The data are presented as the mean ± standard deviation for normally distributed data and as the median (25^{th}, 75^{th} percentiles) for nonnormally distributed data.

Interobserver reliability for the matching of targeted region LN stations was calculated using the kappa statistic. The intraclass correlation coefficient (ICC) was used to measure the interobserver agreement of the evaluation of quantitative parameters. The DLCT quantitative

Table 1 Univariate analysis in the metastatic and nonmetastatic LNs cohorts

Variable	Metastatic LNs cohort (n=58)	Nonmetastatic LNs cohort (n=105)	*t*/Z value	P value
APIC	1.12 (0.80, 1.44)	1.71 (1.45, 2.04)	−7.441	<0.001
APNIC	0.08 (0.06, 0.10)	0.13 (0.11, 0.17)	−7.366	<0.001
APZeff	8.00 (7.78, 8.15)	8.26 (8.14, 8.34)	−7.046	<0.001
APNZeff	0.67±0.03	0.70±0.04	−5.913	<0.001
APλHU	1.39 (1.00, 1.78)	2.12 (1.77, 2.52)	−7.232	<0.001
PVPIC	2.01±0.58	2.41±0.57	−4.276	<0.001
PVPNIC	0.41 (0.31, 0.50)	0.44 (0.39, 0.51)	−1.764	0.078
PVPZeff	8.39±0.27	8.57±0.25	−4.206	<0.001
PVPNZeff	0.88 (0.85, 0.90)	0.88 (0.86, 0.90)	−0.057	0.954
PVPλHU	2.49±0.72	2.93±0.80	−3.460	0.001
L/S	1.50 (1.37, 1.80)	2.06 (1.62, 2.28)	−5.096	<0.001

The data are presented as the mean ± standard deviation and the median (25^{th}, 75^{th} percentiles). LN, lymph node; APIC, iodine concentration in the arterial phase; APNIC, normalized iodine concentration in the arterial phase; APZeff, effective atomic number in the arterial phase; APNZeff, normalized effective atomic number in the arterial phase; APλHU, slope of the spectral attenuation curves in the arterial phase; PVPIC, iodine concentration in the portal venous phase; PVPNIC, normalized iodine concentration in the portal venous phase; PVPZeff, effective atomic number in the portal venous phase; PVPNZeff, normalized effective atomic number in the portal venous phase; PVPλHU, slope of the spectral attenuation curves in the portal venous phase; L/S, nodal ratio of the longest axis to the shortest axis.

parameters and L/S were assessed via the two-sample *t*-test or the Mann-Whitney test. A two-sided P value <0.05 indicated statistical significance. The diagnostic performance of the significant quantitative variables was assessed with the receiver operating characteristic (ROC) curve with 95% confidence interval (CI). The Delong test was applied to evaluate the area under the curve (AUC) of the models, and the cutoff value was determined via the Youden index. The sensitivity and specificity of each significant quantitative parameter were calculated. The same approach was applied to appraise the models that combined the significant DLCT quantitative parameters and L/S, with the model with the best performance being incorporated in a nomogram. A calibration curve was used to evaluate the goodness of fit of the nomogram, and decision curve analysis (DCA) was performed to determine its clinical utility.

Results

Comparison of DLCT quantitative parameters and L/S

The quantitative parameters of DLCT and the L/S in the metastatic and nonmetastatic LN cohorts are summarized in *Table 1*. Except for APNZeff, PVPIC, PVPZeff, and PVPλHU, none of the parameters fit a normal distribution. According to the univariate analysis, the values of APIC, APNIC, APZeff, APNZeff, APλHU, PVPIC, PVPZeff, PVPλHU, and L/S were significantly different between the metastatic and nonmetastatic regional LN cohorts (P<0.001). The κ value for the matching of the targeted regional LN stations was 0.853 (P=0.69), and for all quantitative parameters in the interobserver agreement analysis, the ICC was >0.8. The details are provided in Table S1.

Diagnostic efficacy of DLCT quantitative parameters and L/S

The AUC, sensitivity, and specificity of the quantitative parameters of DLCT and L/S are displayed in *Table 2*. The APIC had the highest diagnostic performance (AUC =0.852; 95% CI: 0.795–0.910), with a sensitivity and specificity of 0.603 and 0.867, respectively. The AUC of L/S was 0.741 (95% CI: 0.659–0.823) under a cutoff value of 1.96, and the sensitivity and specificity for identifying metastatic regional LNs were 0.571 and 0.800, respectively. The ROCs of the quantitative parameters of DLCT and L/S are displayed in *Figure 1*.

Table 2 Diagnostic efficacy of DLCT quantitative parameters and the L/S

DLCT parameter	AUC (95% CI)	Sensitivity	Specificity	Cutoff value
APIC	0.852 (0.795–0.910)	0.603	0.867	1.53
APNIC	0.849 (0.789–0.909)	0.586	0.876	0.11
APZeff	0.834 (0.773–0.894)	0.500	0.905	8.20
APNZeff	0.765 (0.689–0.841)	0.345	0.876	0.67
APλHU	0.843 (0.783–0.902)	0.569	0.867	1.98
PVPIC	0.673 (0.587–0.758)	0.362	0.876	1.65
PVPZeff	0.666 (0.580–0.751)	0.362	0.876	8.30
PVPλHU	0.659 (0.573–0.744)	0.259	0.933	2.23
L/S	0.741 (0.659–0.823)	0.517	0.800	1.96

DLCT, dual-layer detector spectral computed tomography; L/S, nodal ratio of the longest axis to the shortest axis; AUC, area under the curve; CI, confidence interval; APIC, iodine concentration in the arterial phase; APNIC, normalized iodine concentration in the arterial phase; APZeff, effective atomic number in the arterial phase; APNZeff, normalized effective atomic number in the arterial phase; APλHU, slope of the spectral attenuation curves in the arterial phase; PVPIC, iodine concentration in the portal venous phase; PVPZeff, effective atomic number in the portal venous phase; PVPλHU, slope of the spectral attenuation curves in the portal venous phase.

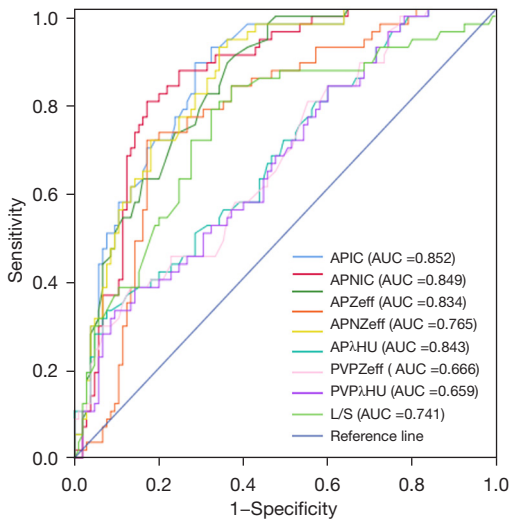

Figure 1 Receiver operating characteristic curves of the DLCT quantitative parameters and L/S for identifying the metastatic regional LNs of PDAC. APIC, iodine concentration in the arterial phase; AUC, area under the curve; APNIC, normalized iodine concentration in the arterial phase; APZeff, effective atomic number in the arterial phase; APNZeff, normalized effective atomic number in the arterial phase; APλHU, slope of the spectral attenuation curves in the arterial phase; PVPIC, iodine concentration in the portal venous phase; PVPZeff, effective atomic number in the portal venous phase; PVPλHU, slope of the spectral attenuation curves in the portal venous phase; L/S, nodal ratio of the longest axis to the shortest axis; DLCT, dual-layer detector spectral computed tomography; LN, lymph node; PDAC, pancreatic ductal adenocarcinoma.

Diagnostic value of the combination of DLCT quantitative parameters and L/S

The AUC, sensitivity, and specificity of the significant DLCT quantitative parameters each combined with L/S are displayed in *Table 3*. The AUCs of these combined models were superior to that of any quantitative parameter alone. The P values of the DeLong test for the AUCs of the DLCT quantitative parameters and L/S as well as those of each DLCT quantitative parameter combined with L/S are displayed in Table S2 and Table S3. The APNIC + L/S model (APNIC-L/S) had the highest diagnostic performance, with an AUC, sensitivity, and specificity of 0.878 (95% CI: 0.825–0.931), 0.707, and 0.886, respectively. The ROCs of the combined models that incorporated each of the significant DLCT quantitative parameters with L/S are displayed in *Figure 2*.

Development and performance of the APNIC-L/S nomogram

The APNIC-L/S nomogram was constructed through a combination of the APNIC and L/S multiplied by their respective weighted coefficients. The ROC of the APNIC-L/S nomogram is displayed in *Figure 3*. The formula was as follows: APNIC-L/S nomogram =6.245–34.687 × APNIC – 1.707 × L/S. The APNIC-L/S nomogram for the identification of metastatic regional LNs of PDAC was established according to the APNIC and L/S model (*Figure 4*). The calibration curve of the nomogram

Table 3 Diagnostic performance of the combined models with DLCT quantitative parameters and the L/S

Combined model	AUC (95% CI)	Sensitivity	Specificity	Cutoff value
APIC + L/S	0.876 (0.822–0.930)	0.690	0.886	0.40
APNIC + L/S	0.878 (0.825–0.931)	0.707	0.886	0.45
APZeff +L/S	0.866 (0.809–0.923)	0.638	0.886	0.32
APNZeff + L/S	0.815 (0.743–0.886)	0.586	0.876	0.46
APλHU + L/S	0.867 (0.810–0.924)	0.690	0.886	0.40
PVPIC + L/S	0.770 (0.696–0.843)	0.397	0.848	0.28
PVPZeff + L/S	0.772 (0.699–0.845)	0.431	0.857	0.27
PVPλHU + L/S	0.763 (0.687–0.838)	0.483	0.848	0.36

DLCT, dual-layer detector spectral computed tomography; L/S, nodal ratio of the longest axis to the shortest axis; AUC, area under the curve; CI, confidence interval; APIC, iodine concentration in the arterial phase; APNIC, normalized iodine concentration in the arterial phase; APZeff, effective atomic number in the arterial phase; APNZeff, normalized effective atomic number in the arterial phase; APλHU, slope of the spectral attenuation curves in the arterial phase; PVPIC, iodine concentration in the portal venous phase; PVPZeff, effective atomic number in the portal venous phase; PVPλHU, slope of the spectral attenuation curves in the portal venous phase.

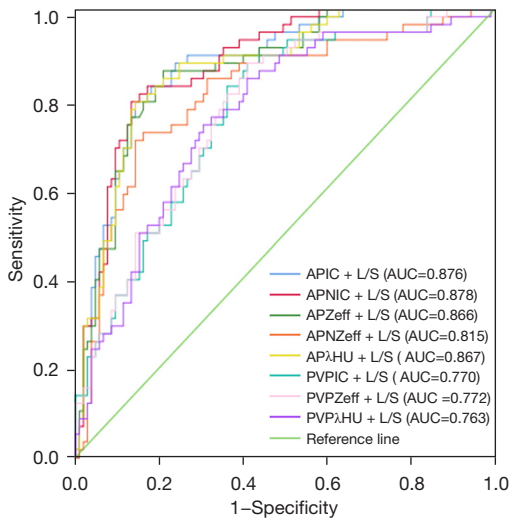

Figure 2 Receiver operating characteristic curves of the combined models with each of the DLCT quantitative parameters and L/S for identifying the regional metastatic LNs of PDAC. APIC, iodine concentration in the arterial phase; L/S, nodal ratio of the longest axis to the shortest axis; AUC, area under the curve; APNIC, normalized iodine concentration in the arterial phase; APZeff, effective atomic number in the arterial phase; APNZeff, normalized effective atomic number in the arterial phase; APλHU, slope of the spectral attenuation curves in the arterial phase; PVPIC, iodine concentration in the portal venous phase; PVPZeff, effective atomic number in the portal venous phase; PVPλHU, slope of the spectral attenuation curves in the portal venous phase; DLCT, dual-layer detector spectral computed tomography; LN, lymph node; PDAC pancreatic ductal adenocarcinoma.

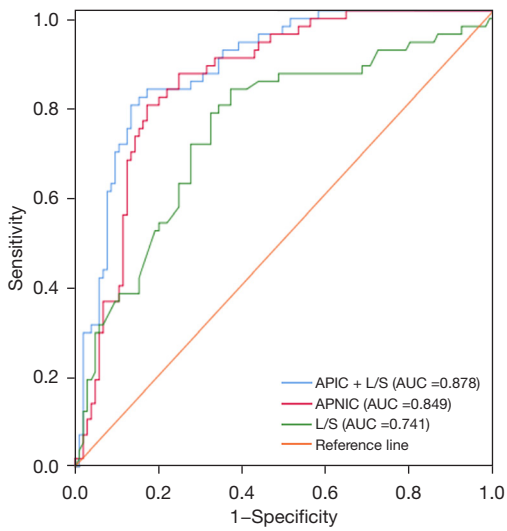

Figure 3 Receiver operating characteristic curves of the APNIC, the L/S, and APNIC + L/S for identifying the metastatic regional LNs of PDAC. APNIC, normalized iodine concentration in the arterial phase; L/S, nodal ratio of the longest axis to the shortest axis; AUC, area under the curve; LN, lymph node; PDAC, pancreatic ductal adenocarcinoma.

demonstrated that the prediction result was in good agreement with the actual observation (*Figure 5*). Moreover, DCA revealed that the nomogram could result in a greater net benefit than could the all-or-none intervention strategy, with threshold probabilities ranging from 0.0 to 0.75 (*Figure 6*). The DLCT images from the metastatic

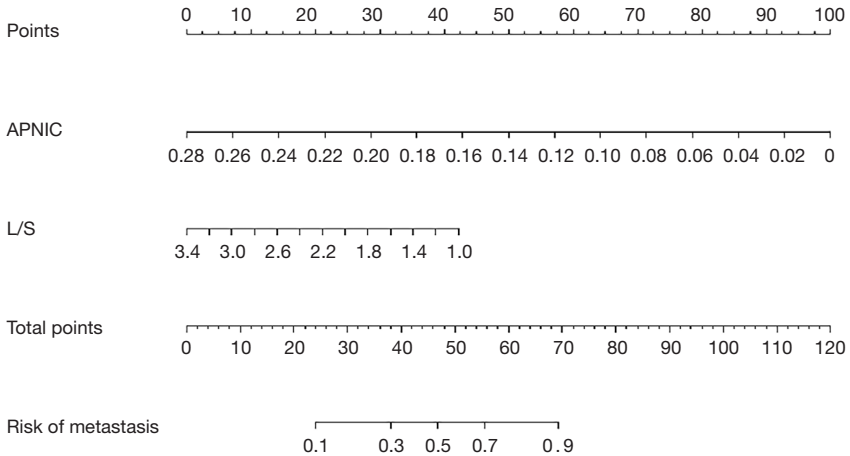

Figure 4 The APNIC-L/S nomogram for assessing the metastatic regional LNs of PDAC. The method for calculating the risk of metastatic regional LNs of PDAC is as follows. (I) Points for each variable are assigned according to corresponding values of the "Points" axis. (II) "Total points" is obtained by summing up the points of all predictors. (III) A vertical line can be drawn down from "Total points" to obtain the risk of metastatic LNs. APNIC, normalized iodine concentration in the arterial phase; L/S, nodal ratio of the longest axis to the shortest axis; LN, lymph node; PDAC, pancreatic ductal adenocarcinoma.

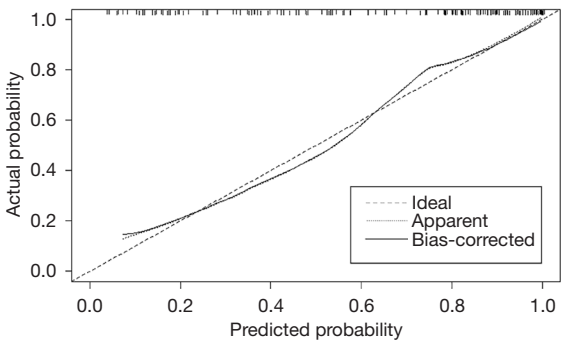

Figure 5 The calibration curve for the APNIC-L/S nomogram. APNIC, normalized iodine concentration in the arterial phase; L/S, nodal ratio of the longest axis to the shortest axis.

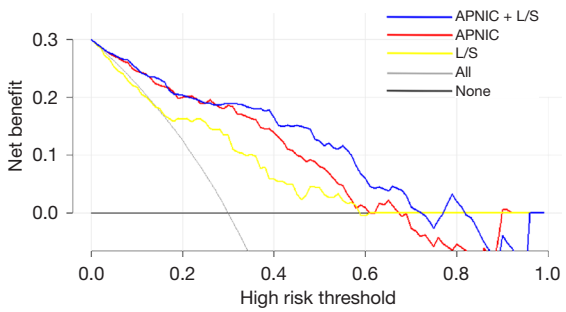

Figure 6 Decision curve analysis of the APNIC-L/S nomogram. The X-axis and the Y-axis represent the high-risk threshold and corresponding net benefit, respectively. The gray line indicates the assumption that all regional LNs are metastatic. The black line represents the assumption that all regional LNs are nonmetastatic. APNIC, normalized iodine concentration in the arterial phase; L/S, nodal ratio of the longest axis to the shortest axis; LN, lymph node.

and nonmetastatic regional LN instances are displayed in *Figures* 7,*8*, respectively.

Discussion

In this study, a nomogram combining quantitative DLCT quantitative parameters and a morphological quantitative indicator for the identification of metastatic regional LNs of PDAC was established and showed good evaluation performance. This finding suggests that DLCT quantitative parameters can be a useful supplement to extant imaging examinations for identifying the metastatic regional LNs of PDAC. In addition, the APNIC-L/S nomogram is easy to use, as it only requires calculating the quantitative parameter APNIC and combining it with the L/S, which is suitable for inexperienced first-line clinicians.

In our study, the quantitative parameters of DLCT including APIC, APNIC, APZeff, APNZeff, APλHU, PVPIC, PVPZeff, PVPλHU, and L/S could independently identify metastatic regional LNs in patients with PDAC. Among these quantitative parameters, the APIC showed

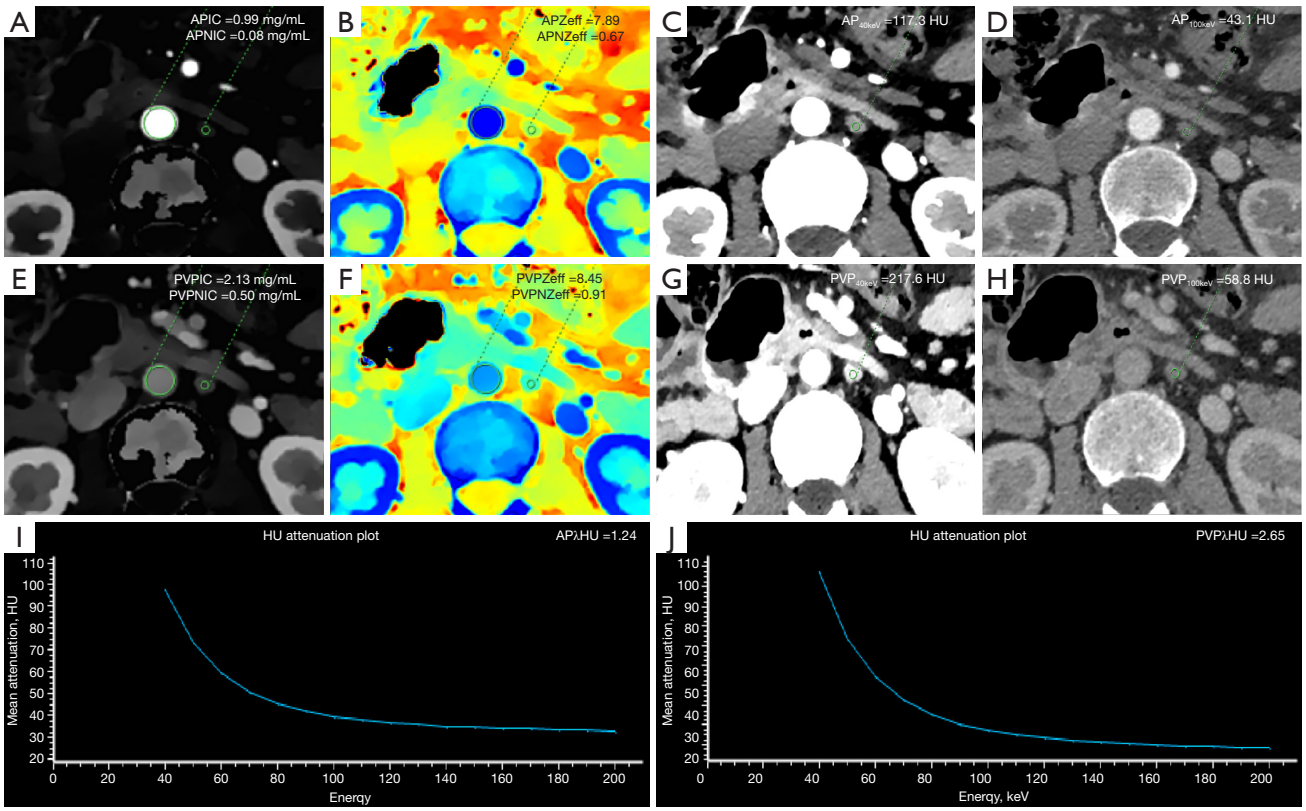

Figure 7 DLCT of a metastatic regional LN in a 56-year-old woman with PDAC. Iodine maps (A,E), effective atomic number (B,F), 40-keV VMI (C,G), 100-keV VMI (D,H), and spectral curve (I,J), with the obtained quantitative parameter values being given for the delineated region of interest (green color). APIC, iodine concentration in the arterial phase; APNIC, normalized iodine concentration in the arterial phase; APZeff, effective atomic number in the arterial phase; APNZeff, normalized effective atomic number in the arterial phase; AP, arterial phase; HU, Hounsfield unit; PVPIC, iodine concentration in the portal venous phase; PVPNIC, normalized iodine concentration in the portal venous phase; PVPZeff, effective atomic number in the portal venous phase; PVPNZeff, normalized effective atomic number in the portal venous phase; PVP, portal venous phase; APλHU, slope of the spectral attenuation curves in the arterial phase; PVPλHU, slope of the spectral attenuation curves in the portal venous phase; DLCT, dual-layer detector spectral computed tomography; LN, lymph node; PDAC, pancreatic ductal adenocarcinoma; VMI, virtual monoenergetic image.

the highest diagnostic efficacy, with an AUC of 0.852. Our findings also revealed that the APIC, APNIC, APZeff, APNZeff, APλHU, PVPIC, PVPZeff, and PVPλHU of metastatic regional LNs were significantly lower than those of nonmetastatic ones. A similar result was confirmed by Liu *et al.* who reported that the mean arterial phase NIC in metastatic LNs was significantly lower than that of nonmetastatic LNs (17). The decline of iodine uptake function may be explained by normal T lymphocytes, B lymphocytes, and other immune cells being replaced after tumor cell invasion, which changes the internal structure of LNs and the X-ray absorption coefficient (22). In addition, tumors with a high degree of malignancy have the characteristics of short doubling, rapid growth, and a significantly increased abundance of new naive blood vessels, which increases the likelihood of necrosis (23,24). In this study, both the APNZeff and APλHU of the metastatic regional LNs were significantly lower than those of the nonmetastatic regional LNs, indicating that the effective atomic number map and spectral curves could similarly help reveal the pathological features of the lesions, which is in line with the findings from experiments reported by Song *et al.* (25).

The diameters of LNs are measured at almost 70 keV in the virtual monoenergetic map because its attenuation value is highly similar to that of conventional 120-kVp CT images, which are familiar to most radiologists. It has been proven that a low-energy image has better subjective

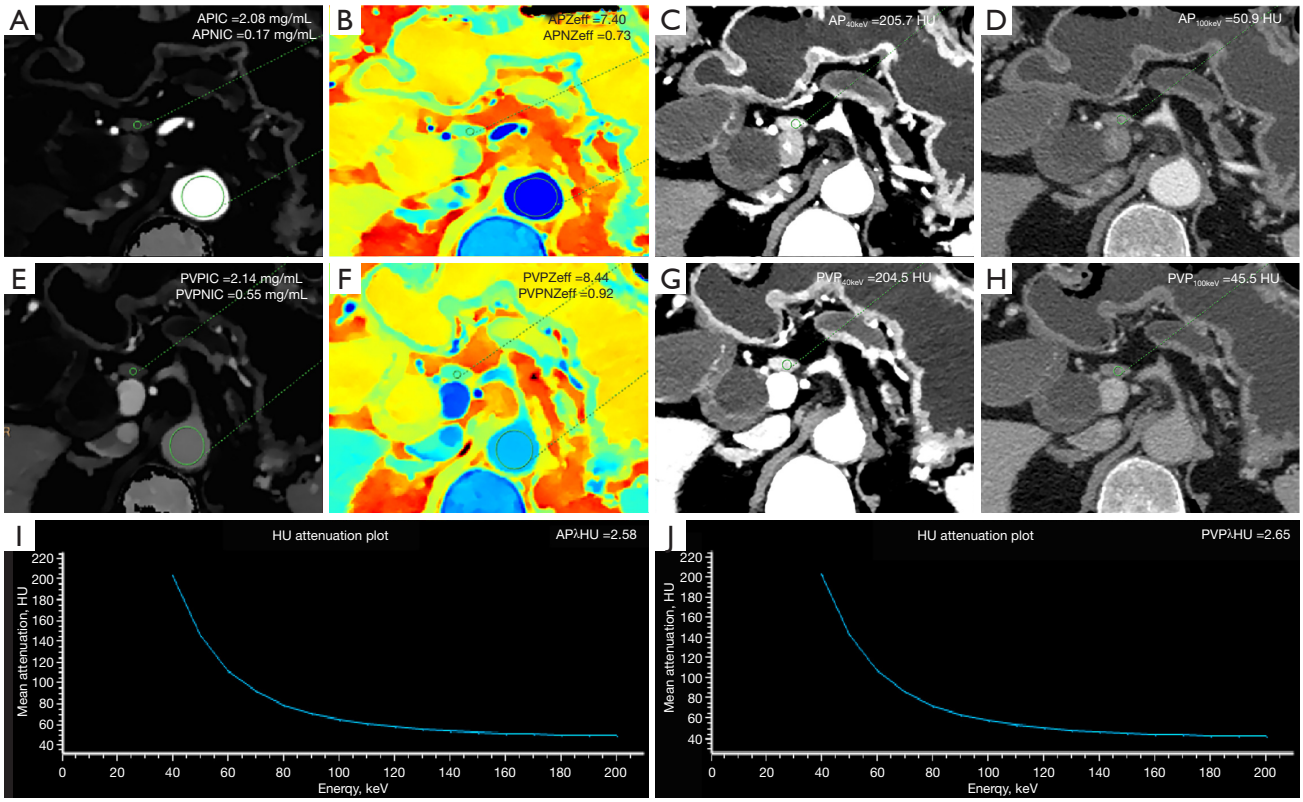

Figure 8 DLCT of a nonmetastatic regional LN in a 71-year-old man with PDAC. Iodine maps (A,E), effective atomic number (B,F), 40-keV VMI (C,G), 100-keV VMI (D,H), and spectral curve (I,J), with the obtained quantitative parameter values being given for the delineated region of interest (green color). APIC, iodine concentration in the arterial phase; APNIC, normalized iodine concentration in the arterial phase; APZeff, effective atomic number in the arterial phase; APNZeff, normalized effective atomic number in the arterial phase; AP, arterial phase; HU, Hounsfield unit; PVPIC, iodine concentration in the portal venous phase; PVPNIC, normalized iodine concentration in the portal venous phase; PVPZeff, effective atomic number in the portal venous phase; PVPNZeff, normalized effective atomic number in the portal venous phase; PVP, portal venous phase; APλHU, slope of the spectral attenuation curves in the arterial phase; PVPλHU, slope of the spectral attenuation curves in the portal venous phase; DLCT, dual-layer detector spectral computed tomography; LN, lymph node; PDAC, pancreatic ductal adenocarcinoma; VMI, virtual monoenergetic image.

and objective image quality than does conventional CT one, with the best energy level and phase being the 40 keV and the portal venous phase (PVP), respectively (26); we therefore chose this energy level and phase to measure the size of LNs, which achieved a high diagnostic efficacy (AUC =0.741). The ratio of the maximal longitudinal to the maximal axial diameter has been recommended as a method for quantifying the shape and the metastatic status of LNs (19). The cutoff value of 1.96 in our study was quite close to the accepted criterion: a ratio of the long axis to the short axis of 2 (27). However, in previous studies, most quantitative indicators of the morphological characteristics of LNs included short-axis diameter (28,29). Consistent with our findings, Liu *et al.* reported that using the axial ratio can significantly improve the sensitivity and positive predictive value of LN diagnosis as compared with using the short-axis diameter, which supports the axial ratio as a reliable indicator for morphological evaluation (20).

Our study also found that as compared to the use of single DLCT quantitative parameters used alone or the single axial-diameter ratio, the combination of DLCT quantitative parameters and morphological features improved the performance for detecting the metastatic regional LNs of the PDAC. The highest diagnostic accuracy was achieved when the APNIC was combined with L/S, which produced an AUC of 0.878 (95% CI: 0.825–0.931), and the sensitivity and specificity were both

the highest among the evaluated models. It is worth noting that although the combination of L/S and APNIC achieved the highest diagnostic efficacy, the sensitivity was still only 0.707. However, the sensitivities of the other models constructed with the combined quantitative parameters of DLCT for predicting LNM tend to range from 0.741 to 0.789 (17,30,31). Gao *et al.* revealed that the quantitative parameters of DLCT combined with morphological information can better reveal the pathological characteristics of metastatic LNs and reflect their internal heterogeneity, demonstrating the added value of combining spectral quantitative parameters (32). On this basis, we constructed a nomogram combining the quantitative DLCT parameter APNIC with the morphological feature L/S, which may assist first-line clinicians in distinguishing PDAC metastatic regional LNs and allow them to make individualized clinical decisions. Finally, this nomogram showed good agreement with the actual pathological results, as shown by the calibration curves. Additionally, this APNIC-L/S nomogram would result in a net benefit in the prediction of metastatic and nonmetastatic risk outcomes, with threshold probabilities ranging between 0.0 and 0.75.

Despite its promising results, several limitations to our study should be noted. Firstly, although we set strict inclusion and exclusion standards, patient selection bias remained due to the retrospective design. Secondly, as data were only collected from a single center, one-to-one correspondence between patient and regional LN could not be achieved due to the small sample size, and it was not possible to incorporate clinical indicators such as carbohydrate antigen 199 for evaluation. Thirdly, although the one-to-one radiology–pathology comparison of regional LNs in PDAC was not achieved, those stations contained both metastatic and nonmetastatic regional LNs were excluded from the study, which ensured that the metastatic status of regional LNs in the target station was consistent. Finally, this is a preliminary exploratory study on the application of the quantitative parameters of DLCT to the metastatic regional LNs of PDAC, and external validation of the APNIC-L/S nomogram will broaden the generality of this model.

Conclusions

This study constructed an APNIC-L/S radiological nomogram consisting of a DLCT quantitative parameter, APNIC, and a morphological quantitative indicator, L/S, which may help to identify metastatic regional LNs in PDAC. This nomogram can help front-line physicians to accurately assess the metastatic status of regional LNs and inform individualized clinical decisions in patients with PDAC.

Acknowledgments

We would like to thank all the volunteers who participated in the study and the staff of the Department of Radiology, Chongqing General Hospital, China, for their selfless and valuable assistance.

Funding: This research was funded by the Medical Research Key Program of both the Chongqing National Health Commission and Chongqing Science and Technology Bureau, China (Nos. 2019ZDXM010 and 2020FYYX151).

Footnote

Reporting Checklist: The authors have completed the TRIPOD reporting checklist. Available at https://qims.amegroups.com/article/view/10.21037/qims-23-1624/rc

Conflicts of Interest: All authors have completed the ICMJE uniform disclosure form (available at https://qims.amegroups.com/article/view/10.21037/qims-23-1624/coif). The authors have no conflicts of interest to declare.

Ethical Statement: The authors are accountable for all aspects of the work in ensuring that questions related to the accuracy or integrity of any part of the work are appropriately investigated and resolved. This retrospective study was approved by the Institutional Review Board of the Chongqing General Hospital (No. KY S2022-075-01) and was conducted in accordance with the Declaration of Helsinki (as revised in 2013). The requirement for informed consent was waived due to the retrospective nature of this study.

References

1. Rahib L, Smith BD, Aizenberg R, Rosenzweig AB, Fleshman JM, Matrisian LM. Projecting cancer incidence and deaths to 2030: the unexpected burden of thyroid, liver, and pancreas cancers in the United States. Cancer Res 2014;74:2913-21.
2. Lin L, Li Z, Yan L, Liu Y, Yang H, Li H. Global, regional, and national cancer incidence and death for 29 cancer groups in 2019 and trends analysis of the global cancer burden, 1990-2019. J Hematol Oncol 2021;14:197.
3. Sung H, Ferlay J, Siegel RL, Laversanne M, Soerjomataram I, Jemal A, Bray F. Global Cancer Statistics 2020: GLOBOCAN Estimates of Incidence and Mortality Worldwide for 36 Cancers in 185 Countries. CA Cancer J Clin 2021;71:209-49.
4. Schneider M, Hackert T, Strobel O, Büchler MW. Technical advances in surgery for pancreatic cancer. Br J Surg 2021;108:777-85.
5. Morales-Oyarvide V, Rubinson DA, Dunne RF, Kozak MM, Bui JL, Yuan C, et al. Lymph node metastases in resected pancreatic ductal adenocarcinoma: predictors of disease recurrence and survival. Br J Cancer 2017;117:1874-82.
6. Dasari BV, Pasquali S, Vohra RS, Smith AM, Taylor MA, Sutcliffe RP, Muiesan P, Roberts KJ, Isaac J, Mirza DF. Extended Versus Standard Lymphadenectomy for Pancreatic Head Cancer: Meta-Analysis of Randomized Controlled Trials. J Gastrointest Surg 2015;19:1725-32.
7. Orci LA, Meyer J, Combescure C, Bühler L, Berney T, Morel P, Toso C. A meta-analysis of extended versus standard lymphadenectomy in patients undergoing pancreatoduodenectomy for pancreatic adenocarcinoma. HPB (Oxford) 2015;17:565-72.
8. Wolfe AR, Prabhakar D, Yildiz VO, Cloyd JM, Dillhoff M, Abushahin L, Alexandra Diaz D, Miller ED, Chen W, Frankel WL, Noonan A, Williams TM. Neoadjuvant-modified FOLFIRINOX vs nab-paclitaxel plus gemcitabine for borderline resectable or locally advanced pancreatic cancer patients who achieved surgical resection. Cancer Med 2020;9:4711-23.
9. Damm M, Efremov L, Birnbach B, Terrero G, Kleeff J, Mikolajczyk R, Rosendahl J, Michl P, Krug S. Efficacy and Safety of Neoadjuvant Gemcitabine Plus Nab-Paclitaxel in Borderline Resectable and Locally Advanced Pancreatic Cancer-A Systematic Review and Meta-Analysis. Cancers (Basel) 2021;13:4326.
10. Facciorusso A, Crinò SF, Muscatiello N, Gkolfakis P, Samanta J, Londoño Castillo J, Cotsoglou C, Ramai D. Endoscopic Ultrasound Fine-Needle Biopsy versus Fine-Needle Aspiration for Tissue Sampling of Abdominal Lymph Nodes: A Propensity Score Matched Multicenter Comparative Study. Cancers (Basel) 2021;13:4298.
11. Wang S, Shi H, Yang F, Teng X, Jiang B. The value of (18)F-FDG PET/CT and carbohydrate antigen 19-9 in predicting lymph node micrometastases of pancreatic cancer. Abdom Radiol (NY) 2019;44:4057-62.
12. Lee JH, Han SS, Hong EK, Cho HJ, Joo J, Park EY, Woo SM, Kim TH, Lee WJ, Park SJ. Predicting lymph node metastasis in pancreatobiliary cancer with magnetic resonance imaging: A prospective analysis. Eur J Radiol 2019;116:1-7.
13. Wunderbaldinger P. Problems and prospects of modern lymph node imaging. Eur J Radiol 2006;58:325-37.
14. Tseng DS, van Santvoort HC, Fegrachi S, Besselink MG, Zuithoff NP, Borel Rinkes IH, van Leeuwen MS, Molenaar IQ. Diagnostic accuracy of CT in assessing extra-regional lymphadenopathy in pancreatic and peri-ampullary cancer: a systematic review and meta-analysis. Surg Oncol 2014;23:229-35.
15. Tawfik AM, Razek AA, Kerl JM, Nour-Eldin NE, Bauer R, Vogl TJ. Comparison of dual-energy CT-derived iodine content and iodine overlay of normal, inflammatory and metastatic squamous cell carcinoma cervical lymph nodes. Eur Radiol 2014;24:574-80.
16. Pan Z, Pang L, Ding B, Yan C, Zhang H, Du L, Wang B, Song Q, Chen K, Yan F. Gastric cancer staging with dual energy spectral CT imaging. PLoS One 2013;8:e53651.
17. Liu H, Yan F, Pan Z, Lin X, Luo X, Shi C, Chen X, Wang B, Zhang H. Evaluation of dual energy spectral CT in differentiating metastatic from non-metastatic lymph nodes in rectal cancer: Initial experience. Eur J Radiol 2015;84:228-34.
18. Le O, Javadi S, Bhosale PR, Koay EJ, Katz MH, Sun J, Yang W, Tamm EP. CT features predictive of nodal positivity at surgery in pancreatic cancer patients following neoadjuvant therapy in the setting of dual energy CT. Abdom Radiol (NY) 2021;46:2620-7.
19. Steinkamp HJ, Hosten N, Richter C, Schedel H, Felix R. Enlarged cervical lymph nodes at helical CT. Radiology 1994;191:795-8.
20. Liu J, Wang Z, Shao H, Qu D, Liu J, Yao L. Improving CT detection sensitivity for nodal metastases in oesophageal cancer with combination of smaller size and lymph node axial ratio. Eur Radiol 2018;28:188-95.
21. Yamada S, Fujii T, Hirakawa A, Kanda M, Sugimoto

H, Kodera Y. Lymph node ratio as parameter of regional lymph node involvement in pancreatic cancer. Langenbecks Arch Surg 2016;401:1143-52.
22. Rizzo S, Radice D, Femia M, De Marco P, Origgi D, Preda L, Barberis M, Vigorito R, Mauri G, Mauro A, Bellomi M. Metastatic and non-metastatic lymph nodes: quantification and different distribution of iodine uptake assessed by dual-energy CT. Eur Radiol 2018;28:760-9.
23. Deniffel D, Sauter A, Dangelmaier J, Fingerle A, Rummeny EJ, Pfeiffer D. Differentiating intrapulmonary metastases from different primary tumors via quantitative dual-energy CT based iodine concentration and conventional CT attenuation. Eur J Radiol 2019;111:6-13.
24. Gao JF, Pan Y, Lin XC, Lu FC, Qiu DS, Liu JJ, Huang HG. Prognostic value of preoperative enhanced computed tomography as a quantitative imaging biomarker in pancreatic cancer. World J Gastroenterol 2022;28:2468-81.
25. Song Z, Li Q, Zhang D, Li X, Yu J, Liu Q, Li Z, Huang J, Zhang X, Tang Z. Nomogram based on spectral CT quantitative parameters and typical radiological features for distinguishing benign from malignant thyroid micronodules. Cancer Imaging 2023;23:13.
26. Nagayama Y, Tanoue S, Inoue T, Oda S, Nakaura T, Utsunomiya D, Yamashita Y. Dual-layer spectral CT improves image quality of multiphasic pancreas CT in patients with pancreatic ductal adenocarcinoma. Eur Radiol 2020;30:394-403.
27. Uematsu T, Sano M, Homma K. In vitro high-resolution helical CT of small axillary lymph nodes in patients with breast cancer: correlation of CT and histology. AJR Am J Roentgenol 2001;176:1069-74.
28. Wu YY, Wei C, Wang CB, Li NY, Zhang P, Dong JN. Preoperative Prediction of Cervical Nodal Metastasis in Papillary Thyroid Carcinoma: Value of Quantitative Dual-Energy CT Parameters and Qualitative Morphologic Features. AJR Am J Roentgenol 2021;216:1335-43.
29. Sun X, Niwa T, Ozawa S, Endo J, Hashimoto J. Detecting lymph node metastasis of esophageal cancer on dual-energy computed tomography. Acta Radiol 2022;63:3-10.
30. Zou Y, Zheng M, Qi Z, Guo Y, Ji X, Huang L, Gong Y, Lu X, Ma G, Xia S. Dual-energy computed tomography could reliably differentiate metastatic from non-metastatic lymph nodes of less than 0.5 cm in patients with papillary thyroid carcinoma. Quant Imaging Med Surg 2021;11:1354-67.
31. Zou Y, Sun S, Liu Q, Liu J, Shi Y, Sun F, Gong Y, Lu X, Zhang X, Xia S. A new prediction model for lateral cervical lymph node metastasis in patients with papillary thyroid carcinoma: Based on dual-energy CT. Eur J Radiol 2021;145:110060.
32. Gao L, Lu X, Wen Q, Hou Y. Added value of spectral parameters for the assessment of lymph node metastasis of lung cancer with dual-layer spectral detector computed tomography. Quant Imaging Med Surg 2021;11:2622-33.

Cite this article as: Wen Y, Song Z, Li Q, Zhang D, Li X, Liu Q, Yu J, Li Z, Ren X, Zhang J, Zeng D, Tang Z. A nomogram based on dual-layer detector spectral computed tomography quantitative parameters and morphological quantitative indicator for distinguishing metastatic and nonmetastatic regional lymph nodes in pancreatic ductal adenocarcinoma. Quant Imaging Med Surg 2024;14(7):4376-4387. doi: 10.21037/qims-23-1624

